DOI: 10.1002/ejic.200800509

Mechanistic Insights into Acetophenone Transfer Hydrogenation Catalyzed by Half-Sandwich Ruthenium(II) Complexes Containing 2-(Diphenylphosphanyl)-aniline – A Combined Experimental and Theoretical Study

Alessia Bacchi,[a] Marcella Balordi,[a][‡] Roberto Cammi,[a] Lisa Elviri,[a] Corrado Pelizzi,[a] Filippo Picchioni,[a] Vincenzo Verdolino,[a] Kees Goubitz,[b] René Peschar,[b] and Paolo Pelagatti*[a]

Keywords: Density functional calculations / Mass spectrometry / Hydrogen transfer / N,P ligands / Ruthenium

Several new half-sandwich ruthenium(II) complexes containing 2-(diphenyphosphanyl)aniline (PNH_2) of formula {Ru[(κ^2P,N)PNH_2](*p*-cymene)Cl}Y [Y = Cl (**1a**), PF_6 (**1b**), BF_4 (**1c**), BPh_4 (**1d**), TfO (**1e**)] were synthesized and fully characterized both in solution (^{1}H NMR and ^{31}P{^{1}H} NMR spectroscopy) and in the solid state (FTIR, X-ray analysis on single crystal). Complexes **1a** and **1b** are active precatalysts in the hydrogen transfer reaction of acetophenone, leading to tof values up to 4440 h^{-1}. In comparison, the {Ru[(κ^2P,N)-$PNMe_2$](*p*-cymene)Cl}Cl complex leads to a tof value of 100 h^{-1} under the same catalytic conditions. The mechanism through which the precatalysts operate was deeply explored by high-resolution MS (ESI) and DFT/PCM studies. The results reveal that the complexes containing PNH_2 operate through a bifunctional mechanism analogous to that proposed for diamines and amino alcohol ligands.

Introduction

Transition-metal complexes containing hybrid amine phosphane ligands, generally indicated as P,N ligands, are among the most studied homogeneous organometallic catalysts.[1] Their success is often attributed to the combination of the soft (P) and hard (N) character of the two donors, which assures a good balance between robustness and reactivity. A well known P,N ligand is 2-(diphenylphosphanyl)-aniline (hereafter referred as PNH_2), whose coordination capability towards several transition-metal ions is known.[2] Usually, PNH_2 chelates the metal in a κ^2P,N way,[2b,2c–3] although κ^1P[2e] and bridging[2a,2e] coordination modes are also reported. Deprotonation of the amine functionality occurs in the presence of a base, giving rise to amido phosphane complexes, where the anionic ligand chelates in a κ^2-P,N way.[3a,3d] Half-sandwich ruthenium(II) complexes containing amino phosphane ligands draw the interest of several groups,[4] especially for their potential catalytic applications.[5] Among these, the hydrogen transfer reaction (HTR) of ketones represents an important example.[6] Recently, Ikariya reported on reduction processes[5e,5g] and racemization of nonracemic *sec*-alcohols[5c] catalyzed by neutral complexes of the type [Cp*Ru(κ^2P,N)Cl], where P,N are several (primary) amino phosphane ligands, PNH_2 included. A metal–ligand bifunctional catalysis[7] has been proposed on the basis of the observation that similar complexes containing (dimethyl)amino phosphane ligands turned completely inactive in the same processes. The presence of NH_2 functionalities is not, however, strictly necessary to construct active precatalysts. Neutral and ionic complexes of the type [(arene)Ru(κ^2P,N)X]$^{n+}$ (arene = Cp or *p*-cymene; P,N = several *N*,*N*-dimethylaminophosphanes; X = CH_3CN, Cl, or Br; *n* = 0, 1) have led from moderate to good activities in the HTR of several ketonic substrates.[5b] Moreover, tof values up to 220000 h^{-1} were reached with the zwitterionic complex [Ru(*p*-cymene)(κ^2P,N)Cl],[5i] where the ligand 1-diisopropylphosphanyl-2-(*N*,*N*-dimethylamino)-1*H*-indene is void of N–H functionalities. In these cases, an inner-sphere mechanism (ISM)[8] seems more likely. On the contrary, Baratta recently demonstrated that precatalysts containing NH_2 functionalities do not automatically operate through an outer-sphere mechanism (OSM) in HTR.[9] Kinetic data and isolation of isopropoxide species suggest in fact that the ruthenium(II) complex [RuCl(CNN)(dppb)] [dppb = $Ph_2P(CH_2)_4PPh_2$; HCNN = 6-(4′-methylphenyl)-2-pyridylmethylamine] works essentially through an ISM, where the NH_2 functionality is, how-

[a] Dipartimento di Chimica Generale ed Inorganica, Chimica Analitica, Chimica Fisica, University of Parma,
Viale G.P. Usberti 17/A, 43100 Parma, Italy
Fax: +39-0521-905557
E-mail: paolo.pelagatti@unipr.it
[b] Laboratory for Crystallography, van't Hoff Institute of Molecular Sciences, Faculty of Sciences, Universiteit van Amsterdam, Valkenierstraat 65, 1018XE Amsterdam, The Netherlands
[‡] Present address: Dipartimento di Chimica Inorganica, Metallorganica, Analitica, University of Milan,
Via Venezian 21, 20133 Milan, Italy
Supporting information for this article is available on the WWW under http://www.eurjic.org or from the author.

ever, involved in the activation of the ketone through N–H···O=C intermolecular hydrogen bonds. To the best of our knowledge, a detailed mechanistic study on the HTR of ketones catalyzed by half-sandwich ruthenium(II) complexes bearing P,N ligands has not yet been reported. For this reason, here we report on the synthesis and characterization of a series of ruthenium(II) complexes of the type {Ru[(κ^2P,N)PNR$_2$](*p*-cymene)Cl}Y (R = H, Me; Y = Cl, PF_6, BF_4, BPh_4, TfO) that have been tested as homogeneous precatalysts for the HTR of acetophenone. A detailed mechanistic study based on MS (ESI), spectroscopic data, and DFT-PCM calculations was carried out in order to elucidate the role played by the NH_2 functionality in the catalytic process.

Results and Discussion

Synthesis of the Ru^{II} Complexes

The reaction between [Ru(*p*-cymene)Cl$_2$]$_2$ with a twofold excess of PNH_2 in dichloromethane at room temperature led to the isolation of a light-orange powder corresponding to the neutral complex {Ru[(κ^1P)PNH_2](*p*-cymene)Cl$_2$} (**1** in Scheme 1).

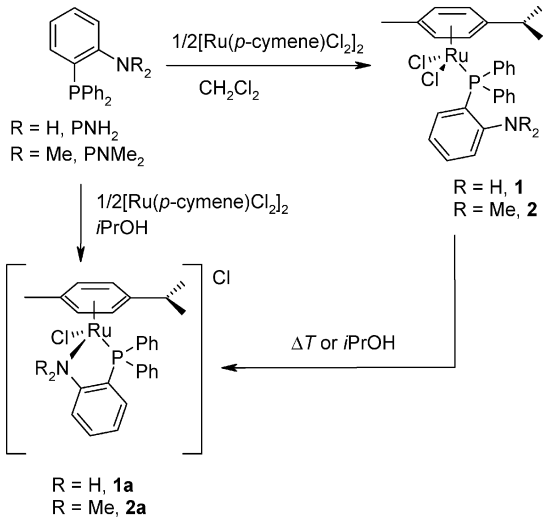

Scheme 1. Synthesis of isomer complexes **1**–**1a** and **2**–**2a**.

PNH_2 uses only the P atom to bind the metal center, with the amine functionality remaining excluded by the coordination sphere. The pseudooctahedral geometry is completed by a η^6-coordinated *p*-cymene ring and by two chloride ligands. The solid structure of **1**, as dichloromethane solvate, was confirmed by X-ray analysis conducted on a single crystal obtained by slow diffusion of *n*-pentane in a dichloromethane solution of **1** (Figure 1).

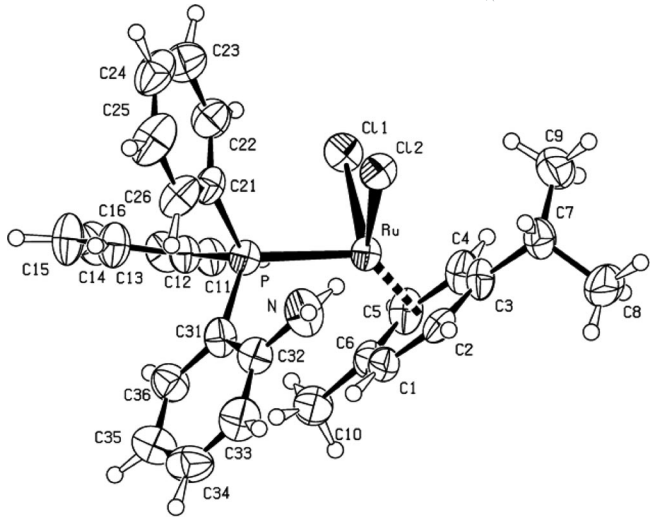

Figure 1. Perspective view and labeling scheme of {Ru[(κ^1P)-PNH_2](*p*-cymene)Cl$_2$} in the crystal structure of **1**·CH_2Cl_2. Thermal ellipsoids drawn at the 50% probability level. Relevant bond lengths [Å] and angles [°] (CM = centroid of the *p*-cymene ring): Ru–P 2.376(2), Ru–Cl1 2.400(2), Ru–Cl2 2.429(2), Ru–CM 1.704; P–Ru–Cl1 88.65(8), Cl1–Ru–CM 124.91(13), Cl2–Ru–CM 125.36(14), P–Ru–CM 130.81(13).

The hexa-hapto coordination of *p*-cymene is regular, with Ru–C distances ranging between 2.18 and 2.25Å. The supramolecular association of **1a**·CH_2Cl_2 in the solid is based on pairing of molecules by means of one bridging chloride atom, interacting by N–H···Cl hydrogen bonds [N1–H1N···Cl2(i) 3.315(3) Å, 133(6)°; N1–H2N···Cl2 3.337(8) Å, 149(5); i = 1 –*x*, –*y*, 1 – *z*]. The coordinated chlorides Cl1 and Cl2 are involved only in long C–H···Cl interactions (>3.34Å) with neighboring phenyl groups. There are also interactions between the solvent molecule and the Cl atoms of the complex [C1S–H11S···Cl1 3.545(10), 143(6); C1S–C12S···Cl2 3.62(2), 155(4)]. The coordination of the ligand through the P donor was confirmed by $^{31}P\{^1H\}$ NMR spectroscopy. The spectrum recorded in deuterated dichloromethane, chloroform, or toluene at room temperature shows a singlet centered at δ = 26 ppm. Under the same conditions, the ^1H NMR signals indicate a certain degree of fluxionality, evidenced by the broadness of the cymene protons that give rise to two signals at δ = 5.46 and 4.84 ppm. The last contains also the amine protons, as established by exchange with deuterated water. In the $^{31}P\{^1H\}$ NMR spectrum recorded in CD_2Cl_2 at 50 °C the signal at δ = 26 ppm is replaced by a new singlet at δ = 56 ppm, which indicates chelation of PNH_2. The deshielding observed upon chelation is a known phenomenon, usually referred as *ring effect* (Δ_R).[10] The amine functionality then replaces a chloride ligand leading to the ionic complex {Ru[(κ^2P,N)PNH_2](*p*-cymene)Cl}Cl (**1a** in Scheme 1).

The ^1H NMR spectrum recorded in CD_2Cl_2 at 50 °C shows strong deshielding of an amine proton as evidenced by the appearance of a new broad singlet at δ = 10.49 ppm, whereas the second amine proton resonates at δ =

5.43 ppm. The same behavior was observed in $CDCl_3$ or $C_6D_5CD_3$. The isomerization **1**→**1a** was also observed after dissolution of **1** in *i*PrOH or after addition of *i*PrOH to a dichloromethane or chloroform solution of **1**.[4c] The behavior observed in *i*PrOH is in agreement with DFT calculations, which evidence how the ring-closure process is favored in *i*PrOH with respect to vacuum (see Computational Details). In all cases, the ring closure was accompanied by a color change of the solution, from orange to yellow. Indeed, when PNH_2 was treated with [Ru(*p*-cymene)Cl_2]$_2$ in *i*PrOH a yellow solution was obtained, from which **1a** was isolated (Scheme 1). Its solid structure was confirmed by X-ray analysis conducted on a single crystal grown by slow diffusion of *n*-pentane in dichloromethane. In **1a**, the {Ru[(κ^2PN)PNH_2](*p*-cymene)Cl}$^+$ cation presents a pseudooctahedral coordination around the metal, constituted by the P,N chelating system, the coordinated chloride anion, and the η^6-*p*-cymene ligand (Figure 2). The complex is chiral, but crystallizes in a centrosymmetric space group, so that both enantiomers (R_{Ru} and S_{Ru}) are present. Chelation of PNH_2 occurs by forming a five-membered ring in an envelope conformation with the ruthenium atom at the flap, deviating by 0.38Å from the ring plane. In fact, this corresponds to the bending by a dihedral angle of 12° of the aniline skeleton with respect to the coordination plane defined by the Ru, P, and N atoms (Figure 2), and it is due to the repulsion between the *p*-cymene methyl group and one phenyl group of PNH_2 (C28···C20 3.30Å).

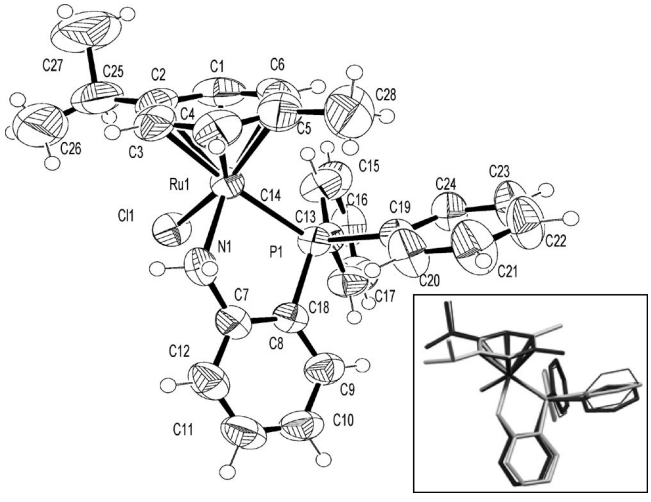

Figure 2. Perspective view and labeling scheme of cation {Ru[(κ^2P,N)PNH_2](*p*-cymene)Cl}$^+$ in the crystal structure of **1a**. Thermal ellipsoids drawn at the 50% probability level. Inset: superposition of {Ru[(κ^2P,N)PNH_2](*p*-cymene)Cl}$^+$ in **1a** (black thick), **1b** (black thin), and **1d**·CH_2Cl_2 (grey thick), hydrogen atoms omitted.[42]

The hexa-hapto coordination of *p*-cymene is regular, with Ru–C distances between 2.16 and 2.26Å. In **1a**, the *p*-cymene is coordinated such that the isopropyl substituent is almost perfectly eclipsed with respect to the chloride ligand [Cl1–Ru1–C2–C25 6.8(5)°]. Solid **1a** slowly decomposes at room temperature, as evidenced by a color change from yellow to green. When PNH_2 was treated with [Ru(*p*-cymene)Cl_2]$_2$ in the presence of halogen scavengers, such as KPF_6, $AgBF_4$, $NaBPh_4$, and AgTfO, the corresponding ionic complexes {Ru[(κ^2P,N)PNH_2](*p*-cymene)Cl}Y [Y = PF_6 (**1b**), BF_4 (**1c**), BPh_4 (**1d**), TfO (**1e**)] were isolated in good yields. The $^{31}P\{^1H\}$ NMR spectra show a singlet centered at 55–56 ppm, in accord with what was seen for **1a**. The solid structures of **1b** and **1d** were solved by X-ray diffraction analysis conducted on single crystals formed upon diffusion of *n*-pentane into dichloromethane solutions of the complexes. The {Ru[(κ^2P,N)PNH_2](*p*-cymene)Cl}$^+$ cation in compound **1b** presents the same geometry as that observed in **1a**, with an rms deviation of 0.27 Å between corresponding atoms in the two structures, mainly due to a slight misorientation of one phenyl ring (Figure 2, inset). In compound **1d**·CH_2Cl_2, {Ru[(κ^2P,N)PNH_2](*p*-cymene)Cl}-BPh_4·CH_2Cl_2, the {Ru[(κ^2P,N)PNH_2](*p*-cymene)Cl}$^+$ cation is isolated as a stereoisomer of the ones observed in **1a**·CH_2Cl_2 and **1b** (Figure 2, inset). The hexa-hapto *p*-cymene ligand is in fact rotated around the bond connecting the metal and the center of mass of the aromatic ring, so that the isopropyl group is no longer eclipsed to the chloride ligand [Cl1–Ru–C2–C25 60.6(3)°], but closer to the NH_2 group [N1–Ru1–C2–C25 –23.6(3)°]. The chelation ring in **1d**·CH_2Cl_2 is perfectly coplanar with the aniline skeleton, because the steric hindrance between the *p*-cymene and the phenyl groups of the phosphane is released by the rotation of the *p*-cymene (C28···C19 3.60Å). The hexa-hapto coordination is regular (Ru–C distances ranging from 2.18 to 2.27Å). Complexes **1c** and **1e** suffer from a somewhat marked instability, both in solution and in the solid state. Contrarily, **1b** and **1d** can be stored under an atmosphere of nitrogen at low temperature for several weeks without decomposition. In solution, however, **1d** tends to decompose more quickly than **1b**, as evidenced by the browning of the solution that occurs within a few hours at room temperature. The reaction between [Ru(*p*-cymene)-Cl_2]$_2$ and a twofold excess of $PNMe_2$ [$PNMe_2$ = 2-(diphenylphosphanyl)-*N*,*N*-dimethylaniline][11] in dichloromethane at room temperature led to the isolation of a brick-red solid, whose elemental analysis is in agreement with the formula [Ru($PNMe_2$)(*p*-cymene)Cl_2] (**2** in Scheme 1). Although literature data are in favor of κ^2P,N chelation,[12] the $^{31}P\{^1H\}$ NMR spectrum of **2** recorded in deuterated chloroform at room temperature shows the presence of two singlets: one centered at δ = 31 ppm and a second one centered at δ = 45 ppm. The first can be assigned to the neutral species {Ru[(κ^1P)$PNMe_2$](*p*-cymene)Cl_2} (**2**), whereas the latter can be assigned to the ionic species {Ru[(κ^2P,N)-$PNMe_2$](*p*-cymene)Cl}Cl (**2a**). The two signals are in a 1:4 ratio. On standing, the solution of **2** at room temperature slowly converted into **2a**, and the isomerization was practically complete within four days. This suggests that in the solid state $PNMe_2$ behaves as κ^1P monodentate ligand. The $^{31}P\{^1H\}$ NMR spectrum of **2** in deuterated *i*PrOH shows only the singlet at δ = 45 ppm indicating the solvent-promoted **2**→**2a** isomerization. The higher chelation degree shown by $PNMe_2$ with respect to PNH_2 is ascribable to the higher nucleophilic character of the amine nitrogen. The

solutions of **2a** are definitively more stable than those containing complexes **1a**–**e**, and color changes or the release of metal particles after several hours at room temperature are not observed.

Catalytic Transfer Hydrogenation

Complexes **1a** and **1b** were selected as precatalysts, *i*PrOH/KOH as the reducing system, and acetophenone as a model substrate. The catalytic activity of complexes **1c**–**e** was not deeply investigated, because of their instability in solution, which impeded satisfactory data reproducibility. All the catalytic reactions were interrupted after 60 min. The catalytic results are collected in Table 1. At room temperature no appreciable formation of 1-phenylethanol was observed. However, when the temperature was increased to 90 °C (oil bath) smooth reduction of acetophenone into 1-phenylethanol occurred, with conversions ranging from 98 to 99% after 1 h of reaction. The catalytic activities of **1a** and **1b** are comparable, with tof values referred to 5 min of 4440 h^{-1} and 3960 h^{-1}, respectively (Table 1, Entries 5 and 6). These values correspond to 37 and 33% conversions, respectively. As can be inferred from Table 1, the precatalysts as well as the presence of KOH are necessary to observe appreciable conversions (Table 1, Entries 1 and 2). The addition of one equivalent of free PNH_2 to a catalytic solution containing **1a** led to deactivation (Table 1, Entry 3), whereas higher concentrations of base blocked the reaction with catalyst decomposition (Table 1, Entry 4). The lower activity of **1b** with respect to that of **1a** seems mainly imputable to the lower stability of the former, as evidenced by the more pronounced browning of the reactant solution containing **1b** within 5 min of reaction. Some of the aforementioned catalytic results allow some mechanistic speculations. For example, the suppression of catalytic activity in the presence of an excess amount of free ligand rules out the possibility that the active catalyst could derive from decomposition of the precatalyst and subsequent formation of the bis(chelate) complex $\{Ru[\kappa^2(P,N)PNH_2]_2Cl_2\}$, which could in principle catalyze the reduction of acetophenone.[13] The suppression of the catalytic activity observed when high concentrations of base are used is instead symptomatic of an OSM.[8,9] The low catalytic activity of **2a**, devoid of N–H functionalities (Table 1, Entry 7), is again symptomatic of an OSM. This implies the formation of two intermediate organometallic cations (vide infra), which are the 16e species $\{Ru[(\kappa^2P,N)PNH](p\text{-cymene})\}^+$ (**IV**) and the 18e hydride $\{Ru[(\kappa^2P,N)PNH_2](p\text{-cymene})H\}^+$ (**V**). Attempts to isolate [**IV**]Y (Y = Cl, PF_6) failed, because of extensive decomposition, with isolation of brown solids difficult to characterize. However, the reaction between **1a** and four equivalents of KOH in refluxing *i*PrOH led to the isolation of a yellow solid, identified as [**V**]Cl. Its ^1H NMR spectrum recorded in deuterated dichloromethane shows in fact a doublet at –8.7 ppm, with $^2J_{HP}$ = 48 Hz.[5e,5i] The $^{31}P\{^1H\}$ NMR spectrum recorded in the same solvent shows a singlet at δ = 67 ppm, whereas the ^{31}P NMR spectrum shows a doublet with $^2J_{HP}$ = 48 Hz. The instability of [**V**]Cl even at low temperatures made its handling difficult. The IR spectrum was necessarily collected by diffuse reflectance technique, that is, sampling directly the solid, as fast decomposition occurred both in KBr and nujol. A limited number of scans was collected, because fast browning of the solid occurred during spectra collection with concomitant fading of the Ru–H stretching band, initially centered at 1933 cm^{-1}.[14] For a more complete characterization of the intermediates involved in the catalytic cycle, we have undertaken a high-resolution MS (ESI) analysis on precatalytic solutions containing complexes **1a** and **1b**. For comparison, the same MS (ESI) study was performed on precatalytic solutions of **2a**.

Table 1. Transfer hydrogenation of acetophenone catalyzed by **1a** and **1b**.[a]

Entry	Complex	Time [min]	Conversion [%][b]	tof [h^{-1}][c]
1	–	60	–	–
2	**1a**[d]	60	–	–
3	**1a**[e]	60	<1	–
4	**1a**[f]	60	<1	–
5	**1a**	5[g]	37	4440
6	**1b**	5[g]	33	3960
7	**2a**	60	10	100

[a] Reactions conditions: refluxing *i*PrOH; acetophenone/Ru/KOH, 1000:1:4; [acetophenone] = 0.1 M. [b] Determined by GC (three independent catalytic experiments). [c] Referred at the reaction time indicated in column 3; *tof* = (mol of product) × (mol Ru)$^{-1}$ × h^{-1}. [d] In the absence of base. [e] Excess amount of free PNH_2. [f] Ru/KOH, 1:10 or 1:20. [g] Conversions ≥98% after 60 min.

MS (ESI) Study

MS (ESI) is a well-suited technique for the transfer of intact charged organometallic fragments from solution to the gas phase, which has been successfully employed for the elucidation of several catalytic mechanisms involving organometallic complexes.[15] We initially analyzed different precatalytic solutions of **1a** and **1b** in different refluxing solvents, such as *i*PrOH, acetonitrile, and THF. A cone voltage (CV) of 10 V was chosen to amplify the softness character of the spectrometric technique, thus avoiding collision-induced dissociations. All the MS (ESI) spectra are collected in the Supporting Information. After 1 h at reflux the precatalysts were preserved, as evidenced by a unique cluster centered at *m*/*z* = 548, corresponding to the expected cation $\{Ru[(\kappa^2P,N)PNH_2](p\text{-cymene})Cl\}^+$ (**III**). When the CV was raised to 30 V a second, a less intense cluster centered at *m*/*z* = 512 appeared, corresponding to the coordinatively unsaturated cationic fragment $\{Ru[(\kappa^2P,N)PNH](p\text{-cymene})\}^+$ (**IV**). This species is generated from **III** upon collision-induced dissociation, thus pointing out the facile HCl releasing form **III**. The MS (ESI) spectra collected with a CV of 10 V after having added an excess amount of KOH to the refluxing *i*PrOH solutions (Ru/KOH, 1:4) show the disappearance of the cluster at *m*/*z* = 548, which is replaced by a cluster at *m*/*z* = 514 corresponding to the cation $\{Ru[(\kappa^2P,N)PNH_2](p\text{-cymene})H\}^+$ (**V**). Lastly, the MS

(ESI) spectra of basic acetonitrile (a non-hydrogen donor) solutions of the precatalysts show a unique cluster centered at m/z = 512 corresponding to **IV**. These results clearly indicate that both complexes operate through an OSM. For comparison, the same MS (ESI) study was conducted on a refluxing *i*PrOH solution of **2a**. With a CV value of 10 V the spectrum shows a unique intense cluster centered at m/z = 576, corresponding to the expected cation $\{Ru[(\kappa^2P,N)PNMe_2](p\text{-cymene})Cl\}^+$. After the addition of KOH (Ru/KOH, 1:4) the above signal is replaced by a cluster centered at m/z = 542, corresponding to the cation $\{Ru[(\kappa^2P,N)PNMe_2](p\text{-cymene})H\}^+$. The formation of **VII** must necessarily occur through a fast β-hydrogen elimination from the undetected alkoxide $\{Ru[(\kappa^2P,N)PNMe_2](p\text{-cymene})(i\text{PrO})\}^+$. This indicates that the low catalytic activity of **2a** is not imputable to the difficulty of forming an hydride species but rather to the difficulty to activate acetophenone. This step must necessary occur through detachment of the amine functionality or partial decoordination of the aromatic ring, steps which appear to be energetically more expensive than the construction of a pericyclic transition state as requested by an OSM (vide infra).

DFT Calculations

HTR of ketones catalyzed by half-sandwich ruthenium(II) complexes in alcoholic media has been deeply investigated by theoretical calculations in order to clarify the intimate steps through which the alcohol and ketone interact with the metal center. Most of these works have been performed on model catalysts containing diamine or amino alcohol ligands,[7,16] whereas to the best of our knowledge, no reports dealing with amine–phosphane based catalysts have so far been reported. Initially we undertook a computational investigation on the conformational stability of **1** in vacuo as well as in *i*PrOH solution to establish the factors governing the ring-closure process observed in solution that transforms **1** into **1a**. Then, the study was directed to the OSM promoted by **1a**, which is hereafter referred to as Path I. In order to have a more complete picture, we also modeled the other two mechanisms deriving from the reactions that $i\text{PrO}^-$ might trigger off by reaction with **1a**, that is, the formation of the isopropoxide intermediate $\{Ru[(\kappa^2P,N)PNH_2](p\text{-cymene})(i\text{PrO})\}^+$ (Path II) and the neutral complex $\{Ru[(\kappa^2P,N)PNH](p\text{-cymene})Cl\}$ (Path III). These two last species would promote the HTR by an ISM. Finally, we compared the corresponding energy profiles to establish the most energetically favored mechanism. In order to have an accurate picture from calculations, the organometallic fragments were built *without* any simplification, and *i*PrOH and acetophenone were used as a hydrogen donor and acceptor, respectively. The energy profiles were determined by calculating the ΔG values as a sum of the electrostatic and nonelectrostatic contributions[17] and a correction for the zero-point energy[18] (for the evolution of the reacting systems see the Supporting Information).

The optimized structures of the precatalyst, reaction intermediates, and transition states are collected in Figure 3. The ring-closure process leading to **1a** (Scheme 1) was studied by DFT calculations in vacuo and in *i*PrOH solution on the basis of Equation (1). Here the organometallic cation $\{Ru[(\kappa^2P,N)PNH_2](p\text{-cymene})Cl\}^+$ is indicated as **III**. All the reagents present in the reactant solution at the onset of the reaction were considered to be present in the initial step. The starting reactants were located at 0.0 kcal/mol energy. This means that neutral complex **1** is located at 0.0 kcal/mol in the energy profile diagram depicted in Figure 4.

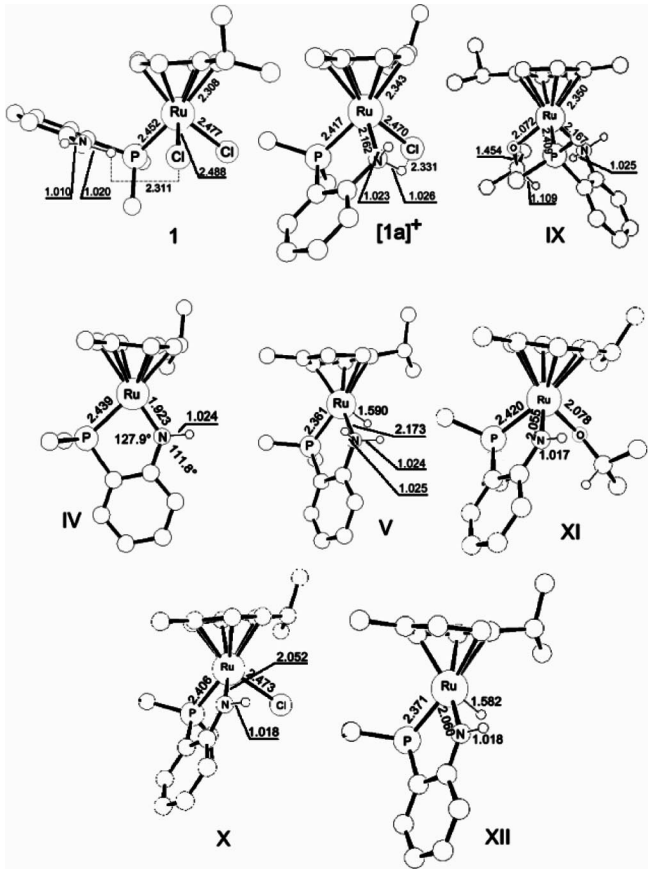

Figure 3. Optimized geometries at B3LYP/BS-0 level of stable intermediate complexes and transition states, related to Paths I and II. For simplicity, hydrogen atoms are omitted except for hydridic and aminic functionalities, whereas the phenyl rings of the phosphane moieties are drawn as single atoms.

$$\mathbf{1} \rightarrow \mathbf{III} + Cl^- \quad (1)$$

The calculations performed in vacuo show an endothermic profile (87.3 kcal/mol) that becomes exothermic once *i*PrOH is introduced into the model (–3.5 kcal/mol, Figure 4). This is in agreement with the experimental observation that the chelation of the PNH_2 ligand occurs easily in *i*PrOH, where cation **III** and anion Cl^- are certainly stabilized, whereas in less-polar solvents the breaking of the Ru–Cl bond is unlikely, and it occurs appreciably only at temperatures ≥50 °C. As can be seen in Figure 3, the chelation leads to a shortening of the Ru–P bond, from 2.452 Å in **1** (2.376Å in the X-ray structure) to 2.417Å in **III**, in accordance with the solid-state structure data of chelate complexes

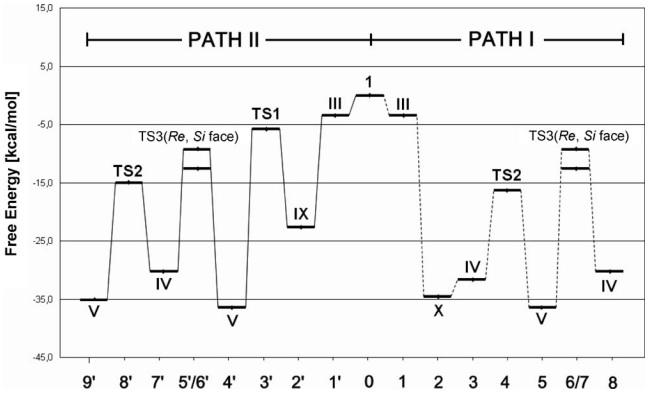

Figure 4. Comparison of the energy profiles of Paths I (on the right) and II (on the left). All the numbered reaction steps are reported as ΔG with respect to **1** and other reactants (see Supporting Information). Only the most important catalytic species are labeled in the graph.

1a, **1b**, and **1d**, where the Ru–P bond lengths are 2.3072, 2.296, and 2.310 Å, respectively. Moreover, an intramolecular hydrogen bond between the axial aminic proton and the coordinated chloride ligand is also found (2.331 Å). Now cation **III** can react with *i*PrO$^-$ by Path I (Scheme 2) or by Path II (Scheme 3). The energy profile of Path I (Figure 4) indicates that the amine deprotonation [Scheme 2, step (*i*)] occurs exothermally with a release of energy of 28.1 kcal/mol. Step (*i*) can be divided into two subsequent steps: amine deprotonation with formation of the transient neutral complex {Ru[(κ^{2}P,N)PNH](*p*-cymene)Cl}[**X**; Scheme 2, step (*ii*)] and chloride dissociation [Scheme 2, step (*iii*)]. The energy difference that separates **X** and **IV** is low (2.9 kcal/mol, Figure 4), pointing out a facile dissociation of the chloride ligand.[19] Structural analysis of the optimized geometry of **IV** shows an evident shortening of the Ru–N bond (1.923Å) with respect to the values found in the complexes crystallographically characterized, in agreement with a substantial amide character of the coordinated nitrogen.

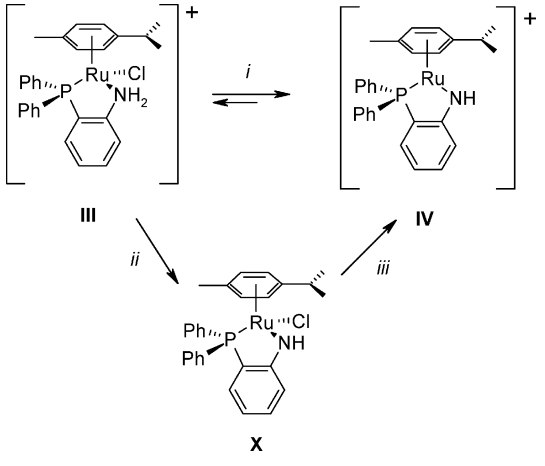

Scheme 2. Path I: deprotonation of the amine functionality with formation of **IV**. Conditions: (*i*) *i*PrO$^-$, –*i*PrOH, –Cl$^-$; (*ii*) *i*PrO$^-$; –*i*PrOH; (*iii*) –Cl$^-$.

This is confirmed by the comparison of the calculated Ru–N–H bond angles in **IV** and **V**, which are 120.2 and

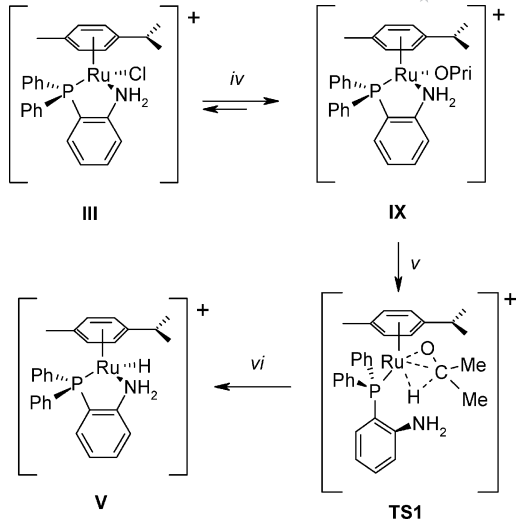

Scheme 3. Reaction steps for Path II. Conditions: (*iv*) *i*PrO$^-$, –Cl$^-$; (*v*) TS for the β-hydrogen elimination step; (*vi*) –Me_2CO.

109.9°, respectively. On the contrary, the calculated Ru–P bond length is sensibly longer in **IV** with respect to those found in the X-ray structures of **1a**, **1b**, and **1d**·CH_2Cl_2 and to that calculated for **V**, passing from 2.408 to 2.305 Å (averaged value) to 2.361 Å, respectively. This elongation could especially explain the difficulty to isolate [**IV**]Y (Y = Cl or PF_6) as a solid, as mentioned above.

In Path II, the first event is the formation of isopropoxide intermediate **IX**, as depicted in Scheme 3 (step *iv*). This step is characterized by a pronounced exothermicity (–19.2 kcal/mol, Figure 4). The subsequent β-hydrogen elimination occurs through **TS1**, where the amine function is not coordinated to ruthenium allowing the formation of an agostic interaction between the α-hydrogen of the alkoxide and ruthenium [Scheme 3, step (*v*)]. This step is quite costly in energy requiring 16.9 kcal/mol with respect to **IX**. The completion of the β-hydrogen elimination leads to hydride **V** and acetone [Scheme 3, step (*vi*)], with a gain in energy of 30.7 kcal/mol with respect to **TS1**. The high exothermicity of the last step implies that once the hydride species is formed the reversed process is strongly unlikely. From an energetic point of view Path II cannot be considered unproductive,[7b] as the required energies do not appear inaccessible. However, the absence of experimental evidences about alkoxide species, as well as the fact that the observed catalytic activities do not increase with base (Table 1, entry 4), suggest that Path I is definitely more likely. Once hydride **V** is formed, the process evolves through Scheme 4. Thus, 16e species **IV** interacts with *i*PrOH through **TS2** [Scheme 4, step (*vii*)]. This step requires 15.3 kcal/mol and leads to **V** and acetone with an exothermic gain of 20.2 kcal/mol. The hydroxy proton is transferred to the nitrogen atom, whereas the C–H proton is transferred to ruthenium [Scheme 4, step (*viii*)], and the whole oxidation of *i*PrOH to acetone gives –4.9 kcal/mol. Now **V** interacts with acetophenone through the pericyclic transition state **TS3** [Scheme 4, step (*ix*)], where the oxygen atom forms a hydrogen bond

with the axial amine proton of **V**, whereas the hydride functionality interacts with the carbonyl carbon atom of the ketone.[20] The simultaneous transfer of the amine proton and hydride ligand to the ketone leads to the formation of **IV** and 1-phenylethanol [Scheme 4, step (*x*)].[21] The 16e species **IV** is 17.6 kcal/mol more stable than **TS3** (considering the *Si* face of acetophenone) and the reduction of acetophenone to 1-phenylethanol needs 6.2 kcal/mol. Thus, the ΔG value of the entire process of oxidation of *i*PrOH and reduction of acetophenone is 1.3 kcal/mol.

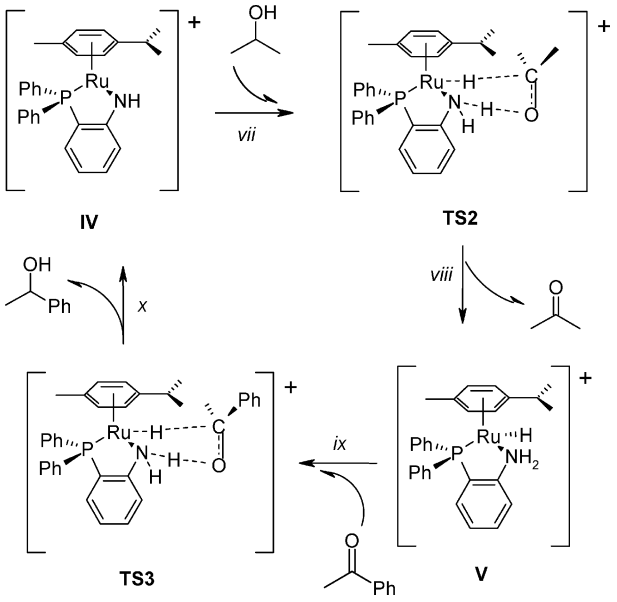

Scheme 4. OSM in action for the reduction of acetophenone catalyzed by **III**. Intermediate **X** has been omitted.

As regards Path III, the optimized geometries of the reactant intermediates and transition states are collected in the Supporting Information. The ground-state intermediates are depicted in Scheme 5. Here we have considered that the initial deprotonation of **1a** gives **X**, *i*PrOH, and Cl^-.

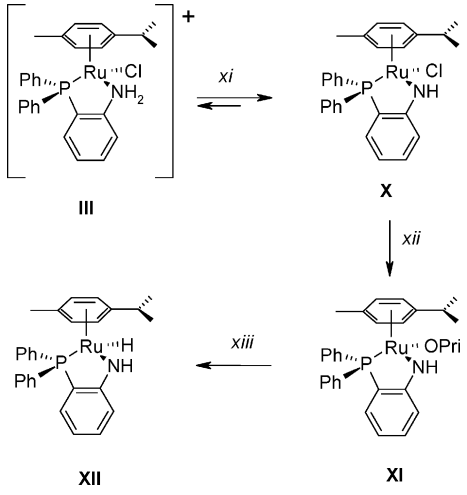

Scheme 5. Reaction steps considered in Path III. Conditions: (*xi*) iPrO$^-$, –*i*PrOH; (*xii*) iPrO$^-$, –Cl$^-$; (*xiii*) –Me_2CO.

Compound **X** reacts with a second iPrO$^-$ ion to give the neutral alkoxide intermediate {Ru[κ^2(P,N)PNH](*p*-cymene)(*i*PrO)} (**XI**), which transforms into the hydride {Ru[κ^2(P,N)PNH](*p*-cymene)H} (**XII**) through β-hydrogen elimination. From an energetic point of view, Path III is much more disfavored than both Path I and Path II. The less likely steps are the formation of hydride **XII** and the activation of acetophenone by **XII**. The first requires in fact the partial decoordination of *p*-cymene, as the amine is covalently bound to the metal, whereas the activation of acetophenone by a pericyclic transition state is hampered by the sp^2 character of the coordinated amide nitrogen atom, which leads to the formation of a strained and then unfavored Ru–H–C–O–H–N ring.

Conclusions

We synthesized several pseudooctahedral Ru^{II} complexes of formula {Ru[(κ^2P,N)PNH_2](*p*-cymene)Cl}Y [Y = Cl (**1a**), PF_6 (**1b**), BF_4 (**1c**), BPh_4 (**1d**), and TfO (**1e**)], which were fully characterized. Complexes **1a** and **1b**, being stable towards decomposition in solution, were investigated as precatalysts in the HTR of acetophenone in basic 2-propanol. The tof values of 4440 and 3960 h^{-1} were obtained for **1a** and **1b**, respectively. On the contrary, complex **2a** {Ru[(κ^2P,N)$PNMe_2$](*p*-cymene)Cl}Cl was much-less active, leading to tof values not higher than 100 h^{-1}.

A detailed mechanistic study based on high-resolution MS (ESI) experiments of precatalytic solutions and DFT/PCM calculations indicates that the catalytic process is governed by a bifunctional mechanism, analogous to that proposed for bis(amine) and amino alcohol ligands.[16e,22] The two active catalytic intermediates are the 16e cation {Ru[(κ^2P,N)PNH](*p*-cymene)}$^+$ (**IV**) and the cationic hydride {Ru[(κ^2P,N)PNH_2](*p*-cymene)H}$^+$ (**V**). DFT/PCM calculations show that the oxidation of *i*PrOH and reduction of acetophenone occur by concerted hydride and proton transfers by pericyclic transition states. Although DFT calculations predict the possibility that **V** could also be formed through β-hydrogen elimination from an alkoxide precursor (Figure 4), experimental evidence supporting this proposal was not collected. The importance of the NH_2 functionality on catalysis is underlined by the low activity of **2a** under the same catalytic conditions. Although the hydride {Ru[(κ^2P,N)$PNMe_2$](*p*-cymene)H} quickly forms in basic *i*PrOH, the activation of acetophenone, likely through detachment of the amine functionality, is hampered. Finally, a mechanism operating through neutral organometallic intermediates of the type {Ru[(κ^2P,N)PNH](*p*-cymene)}(**X**) has been ruled out on the basis of DFT results.

Experimental Section

Materials and Methods: All reactions were carried out under an atmosphere of nitrogen by using standard Schlenk techniques. Solvents were dried according to literature methods and stored over

activated molecular sieves. All reagents were high in purity and used as received. The ligands PNH_2[23] and $PNMe_2$[11] were prepared following literature reported procedures. However, a chromatographic purification, not reported in the original paper, was necessary for PNH_2, which allowed the isolation and identification of {Pd[(κ²P,P)PNP]I_2} (SiO_2, *n*-hexane/ethyl acetate, 9:1 for the elution of the ligand; diethyl ether for the elution of the Pd complex, PNP = {[2-(diphenylphosphane)amino]phenyl}diphenylphosphane)).[24] [Pd(PPh_3)$_4$][25] and [Ru(*p*-cymene)Cl_2]$_2$[26] were prepared by standard procedures. ^{1}H NMR spectra were recorded with AC-300 Bruker or Avance-300 Bruker spectrophotometers, whereas ^{31}P and ^{31}P{^{1}H} NMR spectra were recorded with a AMX-400 Bruker instrument (161.9 MHz for ^{31}P{^{1}H}). Unless otherwise stated, the temperature was 25 °C. IR spectra were collected by means of a Nicolet-Nexus spectrophotometer in the range 4000–400 cm^{-1} from KBr disks or DR (diffuse reflectance) mode. Elemental analyses were performed by using a Carlo Erba 1108 apparatus. The GC analyses were performed by means of a Dani-1000 flame ionization gas chromatograph equipped with a CP Chirasil Dex CB capillary column (25 m length, 0.25 mm i.d.). A quadrupole time-of-flight Micro mass spectrometer (Micromass, Manchester, UK) equipped with a pneumatically assisted ESI interface were used. The system was controlled by Masslynx software version 4.0 (Micromass). The nebulizing gas (nitrogen, 99.999% purity) and the desolvation gas (nitrogen, 99.998% purity) were delivered at a flowrate of 10 and 600 L/h, respectively. The interface parameters were: ESI voltage 3.0 kV, cone voltage 10–30 V, rf lens 0.5 V, source temperature 70 °C, desolvation temperature 70 °C. Continuum mode full-scan mass spectra were acquired over the *m*/*z* = 400–1300 range by using an acquisition time of 1 s and an interscan delay of 0.1 s. QqTOF external calibration was performed by using a 0.1% phosphoric acid solution and a fifth-order nonlinear calibration curve was usually adopted.

Preparation of {Ru[(κ¹P)PNR_2](*p*-cymene)Cl_2} (R = H, 1; R = Me, 2): PNR_2 (0.289 mmol) was dissolved in CH_2Cl_2 (15 mL) at room temperature. [Ru(*p*-cymene)Cl_2]$_2$ (80 mg, 0.131 mmol) dissolved in CH_2Cl_2 (5 mL) was transferred by cannula into the ligand solution, and the resulting orange solution was stirred at room temperature for 2 h. After partial removal of the solvent by vacuum pump, *n*-pentane (5 mL) was added, and the mixture was stored at –18 °C overnight. A yellow-orange powder was collected, which was washed with *n*-hexane and dried under vacuum.

1: Yield: 120 mg (62%). M.p. 228 °C. ^{1}H NMR (300 MHz, CD_2Cl_2): δ = 7.68–7.62 (m, 4 H, Ph), 7.40–7.32 (m, 7 H, Ph), 6.88–6.68 (m, 3 H, Ph), 5.46 (br. s, 2 H, cym), 4.84 (br. s, 4 H, cym, NH_2), 3.07 [sept., 1 H, C*H*(CH_3)$_2$], 1.85 (s, 3 H, CH_3), 1.36 [d, 6 H, CH(C*H*$_3$)$_2$] ppm. ^{31}P{^{1}H} NMR (161.9 MHz, CD_2Cl_2): δ = 28.9 (s) ppm. IR (KBr): $\tilde{\nu}$ = 3363, 3318 (NH_2), 1438 (P–Ph) cm^{-1}. $C_{28}H_{30}Cl_2NPRu{\cdot}CH_2Cl_2$ (668.44): calcd. C 52.14, H 4.79, N 2.10; found C 52.71, H 4.77, N 1.72.

2: Yield: 123 mg (76%). M.p. 152 °C (slow dec.). ^{1}H NMR [300 MHz, $(CD_3)_2CDOD$]: δ = 8.16 (pt, 2 H, Ph), 7.95 (pt, 1 H, Ph), 7.78–7.50 (m, 11 H, Ph), 6.82 (d, $^3J_{HH}$ = 5.8 Hz, 1 H, cym), 6.68 (d, $^3J_{HH}$ = 5.7 Hz, 1 H, cym), 6.47 (br. d, 1 H, cym), 5.44 (d, $^3J_{HH}$ = 5.6 Hz, 1 H, cym), 5.39 (s, 1 H, CH_2Cl_2), 4.15 [s, 3 H, N(CH_3)$_2$], 3.51 [s, 3 H, N(CH_3)$_2$], 3.06 [sept., 1 H, C*H*(CH_3)$_2$], 1.57 (s, 3 H, CH_3), 1.52 [d, $^3J_{HH}$ = 6.7 Hz, 3 H, CH(C*H*$_3$)$_2$], 1.45 [d, $^3J_{HH}$ = 6.8 Hz, 3 H, CH(C*H*$_3$)$_2$] ppm. ^{31}P{^{1}H} NMR (161.9 MHz, CD_2Cl_2): δ = 47.7 (s) ppm. $C_{30}H_{34}Cl_2NPRu{\cdot}1/2CH_2Cl_2$ (654.03): calcd. C 55.75, H 5.94, N 2.11; found C 56.01, H 5.39, N 2.14.

Preparation of {Ru[(κ²P,N)PNH_2](*p*-cymene)Cl}Cl (1a): [Ru(*p*-cymene)Cl_2]$_2$ (50 mg, 0.081 mmol) was dissolved in *i*PrOH (12 mL), and the solution was thermostatted at 82 °C. An *i*PrOH solution (8 mL) of PNH_2 (45 mg, 0.162 mmol) was added by cannula, and the mixture was stirred for 12 h. The final brick-red solution was cooled to room temperature, and the solvent was removed under vacuum. The solid residue was then treated with diethyl ether to obtain a reddish solution and a yellow powder. The supernatant was removed by cannula, and the solid was repeatedly washed with diethyl ether and dried under vacuum. Yield: 94 mg (64%). M.p. 152 °C (dec.). ^{1}H NMR (300 MHz, CD_2Cl_2): δ = 10.49 (s, 1 H, NH), 8.00–7.94 (m, 3 H, Ph), 7.59–7.49 (m, 8 H, Ph), 7.40–7.30 (m, 3 H, Ph), 6.09 (d, 2 H, cym), 5.69 (d, $^3J_{HH}$ = 5.7 Hz, 1 H, cym), 5.31 (d, 1 H, cym), 5.43 (br. s, 1 H, NH), 2.93 [sept., 1 H, C*H*(CH_3)$_2$], 1.78 (s, 3 H, CH_3), 1.27 [d, $^3J_{HH}$ = 6.7 Hz, 3 H, CH(C*H*$_3$)$_2$], 1.23 [d, $^3J_{HH}$ = 6.9 Hz, 3 H, CH(C*H*$_3$)$_2$] ppm. ^{31}P{^{1}H} NMR (161.9 MHz, CD_2Cl_2, 25 °C): δ = 56.3 (s) ppm. IR (KBr): $\tilde{\nu}$ = 3383, 3319, 3215 (NH_2), 1435 (P-Ph) cm^{-1}. The low stability of the solid prevented a correct elemental analysis.

General Procedure for the Preparation of the Ionic Complexes {Ru[(κ²P,N)PNH_2](*p*-cymene)Cl}Y: [Y = PF_6 (1b), BF_4 (1c), BPh_4 (1d), TfO (1e)]: PNH_2 (90 mg, 0.325 mmol) was dissolved in CH_2Cl_2 (30 mL) at room temperature. A CH_2Cl_2 solution (10 mL) of [Ru(*p*-cymene)Cl_2]$_2$ (100 mg, 163 mmol) was added by cannula, and the resulting mixture was stirred until complete dissolution. After the addition of CH_3CN (1 mL), an excess amount of solid halogen scavenger [KPF_6 (**1b**), $AgBF_4$ (**1c**), $NaBPh_4$ (**1d**), AgTfO (**1e**); 1.62 mmol] was added, and the resulting mixture was stirred for 12 h. The solvent was then removed under vacuum, and the solid residue was treated with CH_2Cl_2 (5 mL). After filtration, concentration under vacuum, and refrigeration at –18 °C, a yellow solid was filtered off, which was washed with *n*-hexane and diethyl ether and finally dried under vacuum.

1b: Yield: 57% (130 mg). M.p. 156.8–158.2 °C. ^{1}H NMR (300 MHz, CD_2Cl_2): δ = 7.92 (m, 2 H, Ph), 7.76 (m, 1 H, Ph), 7.63–7.44 (m, 9 H, Ph), 7.18 (m, 2 H, Ph), 6.83 (br. d, 1 H, N-H), 5.75 (pt, 2 H, cym), 5.67 (br. s, 1 H, N-H), 5.61 (d, $^3J_{HH}$ = 5.7 Hz, 1 H, cym), 5.40 (d, $^3J_{HH}$ = 5.4 Hz, 1 H, cym), 2.53 [sept., 1 H, C*H*(CH_3)$_2$], 1.77 (s, 3 H, CH_3), 1.18 [d, $^3J_{HH}$ = 6.9 Hz, 3 H, CH(C*H*$_3$)$_2$], 1.11 [d, $^3J_{HH}$ = 6.9 Hz, 3 H, CH(C*H*$_3$)$_2$] ppm. ^{31}P{^{1}H} NMR (161.9 MHz, CD_2Cl_2): δ = 57 (s, PNH_2), –141 (sept., PF_6) ppm. IR (DR): $\tilde{\nu}$ = 3292 (NH_2), 1438 (P–Ph), 843 (P–F) cm^{-1}. $C_{28}H_{30}ClF_6NP_2Ru{\cdot}1/4CH_2Cl_2$ (714.25): calcd. C 48.11, H 4.33, N 1.99; found C 47.56, H 4.28, N 2.15. By slow diffusion of *n*-pentane into a dichloromethane solution of the complex, X-ray quality crystals were collected.

1c: Yield: 69% (59 mg). ^{1}H NMR (300 MHz, CD_2Cl_2): δ = 7.69–7.27 (m, 14 H, Ph), 6.99 (br. d, 1 H, N-H), 6.52 (br. d, 1 H, N-H), 6.04 (m, 2 H, cym), 5.92 (d, $^3J_{HH}$ = 6.0 Hz, 1 H, cym), 5.78 (d, $^3J_{HH}$ = 5.5 Hz, 1 H, cym), 2.62 [sept., 1 H, C*H*(CH_3)$_2$], 1.82 (s, 3 H, CH_3), 1.16 [d, $^3J_{HH}$ = 6.0 Hz, 3 H, CH(C*H*$_3$)$_2$], 1.08 [d, $^3J_{HH}$ = 6.0 Hz, 3 H, CH(C*H*$_3$)$_2$] ppm. ^{31}P{^{1}H} NMR (161.9 MHz, CD_2Cl_2): δ = 58 (s) ppm. IR (DR): $\tilde{\nu}$ = 3242 (NH_2), 1445 (P–Ph), 813 (B-F) cm^{-1}. The instability of the complex prevented correct elemental analysis and the recording of the m.p.

1d: Yield: 89% (395 mg). M.p. 145 °C. ^{1}H NMR (300 MHz, CD_2Cl_2): δ = 7.94 (pt, 1 H, Ph), 7.60–7.38 (m, 9 H, Ph), 7.27–7.17 (m, 12 H, Ph), 7.00–6.96 (m, 8 H, Ph), 6.85–6.81 (m, 5 H, Ph), 6.70 (br. s, 1 H, N-H), 6.19 (br. s, 1 H, N-H), 5.70 (m, 2 H, cym), 5.46 (m, 2 H, cym), 2.53 [sept., 1 H, C*H*(CH_3)$_2$], 1.66 (s, 3 H, CH_3), 1.14 [d, $^3J_{HH}$ = 6.0 Hz, 3 H, CH(C*H*$_3$)$_2$], 1.04 [d, $^3J_{HH}$ = 6.0 Hz, 3 H, CH(C*H*$_3$)$_2$] ppm. ^{31}P{^{1}H} NMR (161.9 MHz, CD_2Cl_2): δ = 58 (s) ppm. IR (KBr): $\tilde{\nu}$ = 3238, 3194 (NH_2), 1445 (P–Ph), 843 (B–Ph) cm^{-1}. $C_{52}H_{50}BClNPRu{\cdot}CH_2Cl_2$ (952.22): calcd. C 66.85, H 5.50, N

1.47; found C 66.75, H 5.33, N 1.50. By slow diffusion of *n*-pentane into a dichloromethane solution of **1d** crystals suitable for X-ray analysis were collected.

1e: Yield: 25% (74 mg). M.p. 130 °C (dec.). ^{1}H NMR (300 MHz, [D$_8$]THF): δ = 8.29 (br. d, 1 H, N-H), 8.09 (pt, 2 H, Ph), 7.71–7.30 (m, 12 H, Ph), 6.98 (br. d, 1 H, N-H), 6.08 (d, $^3J_{HH}$ = 6.1 Hz, 1 H, cym), 5.89 (d, $^3J_{HH}$ = 6.1 Hz, 1 H, cym), 5.74 (d, $^3J_{HH}$ = 6.0 Hz, 1 H, cym), 5.66 (d, $^3J_{HH}$ = 6.0 Hz, 1 H, cym), 2.79 [sept., 1 H, C*H*(CH$_3$)$_2$], 1.60 (s, 3 H, CH$_3$), 1.21 [pt, 6 H, CH(C*H*$_3$)$_2$] ppm. ^{31}P{^{1}H} NMR (161.9 MHz, [D$_8$]THF): δ = 56 (s) ppm. IR (DR): $\tilde{\nu}$ = 3320 (NH$_2$), 1430 (P–Ph), 1024 (S–O) cm^{-1}. The instability of the complex precluded a correct elemental analysis.

[V]Cl: Compound **1** (10 mg, 0.017 mmol) was dissolved in *i*PrOH (5 mL) and then KOH (4 equiv.) was added. The solution was the heated at reflux for not more than 60 min. The final yellow-brown solution was passed through sintered glass, and the resulting yellow solution quickly dried under vacuum to release a yellow powder. ^{1}H NMR (300 MHz, CD_2Cl_2): δ = 7.90 (m, 2 H, Ph), 7.41 (m, 8 H, Ph), 6.97 (pt, $^3J_{HH}$ = 9 Hz, 1 H, Ph), 6.7 (pt, $^3J_{HH}$ = 8.1 Hz, 1 H, Ph), 6.33 (m, $^3J_{HH}$ = 7 Hz, 1 H, Ph), 6.00 (pt, $^3J_{HH}$ = 7 Hz, 1 H, Ph), 5.30 (d, 1 H, cym, overlapped with CD_2Cl_2), 5.05 (d, $^3J_{HH}$ = 5.7 Hz, 1 H, cym), 4.97 (d, $^3J_{HH}$ = 6 Hz, 1 H, cym), 4.84 (d, $^3J_{HH}$ = 5.7 Hz, 1 H, cym), 3.48 (br. s, 2 H, NH$_2$), 2.33 [sept., 1 H, C*H*(CH$_3$)$_2$], 1.82 (s, 3 H, CH$_3$), 1.16 [d, 3 H, CH(C*H*$_3$)$_2$ overlapped with residual *i*PrOH], 1.13 [d, $^3J_{HH}$ = 6.9 Hz, 3 H, CH(C*H*$_3$)$_2$] ppm. ^{31}P{^{1}H} NMR (161.9 MHz, CD_2Cl_2): δ = 67 (s) ppm. ^{31}P NMR (400 MHz, CD_2Cl_2): δ = 67 (d, $^2J_{HP}$ = 48 Hz) ppm. IR (DR): $\tilde{\nu}$ = 3400 (NH$_2$), 1933 (Ru–H), 1435 (P–Ph) cm^{-1}. The high instability of the solid prevented determination of the yield, m.p., and elemental analysis.

X-ray Crystallographic Analysis: Crystal data collection and structure determination results are given in Table 2. For complex **1**, data collection was performed with an Enraf–Nonius CAD-4 diffractometer with graphite-monochromated Cu-K_α radiation and ω-2θ scan. Corrections for Lorentz and polarization effects were applied. Absorption correction was performed with the program PLATON,[27] following the method of North et al.[28] by using Ψ-scans of five reflections, with coefficients in the range 0.731–0.942. The structure was solved by the PATTY option of the DIRDIF-99[29] program system. After isotropic refinement of the initial model, a difference Fourier map revealed 3 peaks that were interpreted as belonging to CH_2Cl_2, one of the solvents used during crystallization. The hydrogen atoms were calculated. Full-matrix least-squares refinement on F, anisotropic for the non-hydrogen atoms, and isotropic for the hydrogen atoms, restraining the latter in such a way that the distance to their carrier remained constant at approximately 1.0 Å and with a fixed atomic displacement parameter of u = 0.08Å^2, converged to R = 0.072, R_w = 0.079, $(\Delta/\sigma)_{max}$ = 0.06, S = 1.02. A weighting scheme was used. The secondary isotropic extinction coefficient refined to g = 2(38).[30] A final difference Fourier map revealed a residual electron density between –2.16 and 2.23 e Å^{-3} in the vicinity of the heavy atom. Scattering factors were taken from Cromer and Mann.[31] The anomalous scattering of Ru, Cl, and P was taken into account.[32] All calculations were performed with XTAL3.7,[33] unless otherwise stated. Mo-K_α radiation (λ = 0.71073 Å), T = 293 K with a SMART AXS 1000 CCD diffractometer for compounds **1a**, **1b**, and **1d**·CH_2Cl_2. Lorentz, polarization, and absorption corrections were applied.[34] Structures were solved by direct methods by using SIR97[35]and refined by full-matrix least-squares on all F^2 by using SHELXL97[36] implemented in the WingX package.[37] Hydrogen atoms partly located on Fourier difference maps and refined isotropically and partly introduced in calculated positions. Anisotropic displacement parameters refined for all non-hydrogen atoms. Hydrogen bonds were analyzed with SHELXL97[36] and PARST97,[38] and extensive use was made of the Cambridge Crystallographic Data Centre packages[39]for the analysis of crystal packing.

CCDC-673489 (for **1**·CH_2Cl_2), -673490 (for **1a**), -673491 (for **1b)**, -673492 (for **1d**·CH_2Cl_2), and -673493 {for Pd[(κ^2P,P)PNP]I$_2$} contain the supplementary crystallographic data for this paper. These data can be obtained free of charge from The Cambridge Crystallographic Data Centre via www.ccdc.cam.ac.uk/data_request/cif.

Table 2. Crystal data and structure refinement for **1**·CH_2Cl_2, **1a**, **1b**, and **1d**·CH_2Cl_2.

	1·CH_2Cl_2	**1a**	**1b**	**1d**·CH_2Cl_2
Formula	$C_{29}H_{32}Cl_4NPRu$	$C_{28}H_{30}Cl_2NPRu$	$C_{28}H_{30}ClF_6NP_2Ru$	$C_{53}H_{52}BCl_3NPRu$
Formula weight	668.4	583.47	692.99	952.16
Wavelength [Å]	1.5418	0.71073	0.71073	0.71073
a [Å]	9.383(2)	11.1548(6)	11.088(2)	14.710(1)
b [Å]	13.317(5)	14.8570(8)	11.816(2)	18.427(1)
c [Å]	13.401(5)	16.7902(9)	22.556(4)	18.163(1)
a [°]	71.05(3)	90	90	90
β [°]	77.29(3)	105.069(1)	97.762(3)	102.2680(10)
γ [°]	70.37(3)	90	90	90
V [Å^3]	1480.1(9)	2686.9(3)	2928.1(9)	4810.9(5)
Crystal system	Triclinic	Monoclinic	07monoclinic	Monoclinic
Space group	$P\bar{1}$	P 2$_1$/n	P 2$_1$/n	P 2$_1$/n
Z	2	4	4	4
D_x [g cm^{-3}]	1.50	1.442	1.572	1.315
Abs. coeff.	8.26	0.858	0.793	0.561
F(000)	680	1192	1400	1968
θ range [°]	3.5–74.9	1.86–27.50	1.82–23.31	1.59–26.38
Meas. refls.	6084	32500	19944	52744
Ind. refls. [*R*(int)]	6084	6160 [0.0490]	4220 [0.0727]	9819 [0.0350]
Data/restr./param.	5112/0/422	6160/0/309	4220/536/307	9819/0/552
Final R_1,$wR_2[I>2\sigma(I)]$	0.072/0.079	0.0378, 0.0873	0.1272, 0.2965	0.0358, 0.0980
Goodness-of-fit on F^2	1.02	0.870	1.300	1.014
ΔF (max, min) [e Å^{-3}]	2.23, –2.23	0.643, –0.350	1.715, –2.624	0.838, –0.647

Catalytic HTR: By way of an example, the acetophenone reduction catalyzed by **1a** is reported. Compound **1** (2.5 mg, 4.284×10^{-3} mmol) was introduced into a 200-mL capacity Schlenk reactor equipped with a magnetic bar. The vessel was evacuated and refilled with nitrogen at least three times. Then, dry *i*PrOH (42 mL) was introduced by cannula, and the solution was thermostatted at 90 °C (oil bath) for 1 h. During the warming period, the solution turned from orange to yellow indicating the isomerization of **1** into **1a**. After the addition of a KOH solution (0.29 M in *i*PrOH, 60 μL) the stirring was maintained for another 30 min before acetophenone (500 μL, 4.284 mmol) was added. The final concentration of ruthenium in the reactant solution was 10^{-4} M, whereas the final concentration of acetophenone was 0.1 M. Four subsequent samples (0.5 mL) were withdrawn after 5, 15, 30, and 60 min. Each sample was passed through a short silica column in order to remove the metal (diethyl ether as eluent) and then treated with water and extracted with diethyl ether (3×). After drying with anhydrous sodium sulfate and filtering, the samples were analyzed by GC.

MS (ESI) Experiments: The solutions were prepared as described for the catalytic runs. Aliquots of the reactant solutions were withdrawn and immediately analyzed by direct infusion into the ESI source equipped with a Qq-TOF high-resolution MS spectrometer. All the experimental isotope clusters were in agreement with the theoretical masses and with the reconstructed singly charged ESI isotope patterns.

Computational Details: The geometries of all minimums and saddle points were optimized in the gas phase at density functional theory (DFT) level by means of hybrid B3LYP functional.[40] For geometry optimization D95V (H, C, N, O) and ECP plus DZ (P, Cl, Ru) basis sets were used (BS-0). Thermochemical analysis was performed on all intermediates and unique imaginary frequencies searched in transition states. Accurate energy calculation was performed on gas-phase optimized geometry at B3LYP level in solvent environment simulation by using integral formalism polarizable continuum model (IEF-PCM) at five different basis set levels: (a) BS-0; (b) 6-31G (H, C, N, O) and ECP plus DZ (P, Cl, Ru) (BS-I); (c) 6-31G(d,p) (H, C, N, O, P, Cl) and ECP plus DZ (Ru) (BS-II); (d) 6-31G(d,p) (H, C, N, O, P, Cl) and ECP plus DZ (Ru) (BS-III); (e) 6-31++G(d,p) (H, C, N, O, P, Cl) and ECP plus DZ (Ru) (BS-IV), see Supporting Information. Only BS-IV results are reported, because different levels of accuracy did not show important variation in the qualitative and quantitative description of the catalytic cycle. The PCM parameters are: Ua0 model for building of cavities, dielectric constant fixed to 18.3, density of the medium equal to 0.007876 particle/Å^{-3} and 0.3 Å^{-2} the areas of tesserae. Additional spheres were added on acid hydrogens. All the calculations were performed with the Gaussian03 package.[41]

Supporting Information (see footnote on the first page of this article): Crystal data, structure refinement, and ORTEP view of {Pd[(κ^2P,P)PNP]I_2}; MS (ESI) spectra of the precatalytic solutions; reaction steps considered in the evaluation of the ΔG values of the reaction paths; free energy data in Hartree comprehensive of electrostatic, repulsive, dispersive, and cavitation energy of the intermediates of Path I–III; zero-point energy correction in Hartree computed on the gas-phase optimized geometry; number of imaginary modes and relative frequencies in cm^{-1} of the most important transition states found in Paths I–III; optimized geometries of intermediates and transition states located for Path III.

[1] a) E. Drent, P. Arnoldy, P. H. M. Budzelaar, *J. Organomet. Chem.* **1993**, *455*, 247–253; b) P. Denis, A. Jean, J. F. Croizy, A. Mortreux, F. Petit, *J. Am. Chem. Soc.* **1990**, *112*, 1292–1294; c) T. B. Rauchfuss, J. L. Clements, S. F. Angew, D. M. Roundhill, *Inorg. Chem.* **1977**, *16*, 775–778; d) M. Koprovski, R.-S. Sebastián, V. Maraval, M. Zablocka, V. Cadierno, B. Donnadieu, A. Igau, A.-M. Caminade, J.-P. Majoral, *Organometallics* **2002**, *21*, 4680–4687; e) J.-D. Huang, X.-P. Hu, S.-B. Yu, J. Deng, D.-Y. Wang, Z.-C. Duan, Z. Zheng, *J. Mol. Catal. A Chem.* **2007**, *270*, 127–131; f) P. Cheruku, S. Gohil, P. G. Andersson, *Org. Lett.* **2007**, *9*, 1659–1661; g) J. Andrieu, J. M. Camus, P. Richard, R. Poli, L. Gonsalvi, F. Vizza, M. Peruzzini, *Eur. J. Inorg. Chem.* **2006**, 51–61.

[2] a) C. J. Adams, M. I. Bruce, B. W. Skelton, A. H. White, *J. Organomet. Chem.* **1996**, *513*, 255–271; b) L. Crociani, R. Anacardio, P. Traldi, B. Corain, *Inorg. Chim. Acta* **1998**, *282*, 119–122; c) L. Crociani, F. Tisato, F. Refosco, G. Bandoli, B. Corain, *Eur. J. Inorg. Chem.* **1998**, 1689–1697; d) M. B. Smith, A. M. Z. Slawin, *New J. Chem.* **2000**, *24*, 65–67; e) O. Crespo, E. J. Fernández, M. Gil, M. C. Gimeno, P. G. Jones, A. Laguna, J. M. López-de-Luzuriaga, M. E. Olmos, *J. Chem. Soc., Dalton Trans.* **2002**, 1319–1326.

[3] a) L.-C. Liang, *Coord. Chem. Rev.* **2006**, *250*, 1152–1177; b) K. R. Reddy, K. Surekha, G.-H. Lee, S. M. Peng, S.-T. Liu, *Organometallics* **2000**, *19*, 2637–2639; c) L. Dahlenburg, K. Herbst, A. Zahl, *J. Organomet. Chem.* **2000**, *616*, 19–28; d) K. R. Reddy, W. W. Tsai, K. Surekha, G.-H. Lee, S.-M. Peng, J.-T. Chen, S.-T. Liu, *J. Chem. Soc., Dalton Trans.* **2002**, 1776–1782; e) H.-Y. Wang, G.-X. Jin, *Eur. J. Inorg. Chem.* **2005**, 1665–1670.

[4] a) R. Morris, A. Habtemariam, Z. Guo, S. Parsons, P. J. Sadler, *Inorg. Chim. Acta* **2002**, *339*, 551–559; b) M. A. Rankin, R. McDonald, M. J. Ferguson, M. Stradiotto, *Organometallics* **2005**, *24*, 4981–4994; c) C. G. Arena, S. Calamia, F. Faraone, C. Graiff, A. Tiripicchio, *J. Chem. Soc., Dalton Trans.* **2000**, 3149–3157.

[5] a) K. Mauthner, C. Slugovc, K. Mereiter, R. Schmid, K. Kirchner, *Organometallics* **1997**, *16*, 1956–1961; b) C. Standfest-Hauser, C. Slugovc, K. Mereiter, R. Schmid, K. Kirchner, L. Xiao, J. Weissensteiner, *J. Chem. Soc., Dalton Trans.* **2001**, 2989–2995; c) M. Ito, A. Osaku, S. Kitahara, M. Hirakawa, T. Ikariya, *Tetrahedron Lett.* **2003**, *44*, 7521–7523; d) C. Thoumazet, M. Melaimi, L. Ricard, F. Mathey, P. Le Floch, *Organometallics* **2003**, *22*, 1580–1581; e) M. Ito, M. Hirakawa, A. Osaku, T. Ikariya, *Organometallics* **2003**, *22*, 4190–4192; f) M. Ito, S. Kitahara, T. Ikariya, *J. Am. Chem. Soc.* **2005**, *127*, 6172–6173; g) M. Ito, A. Sakaguchi, C. Kobayashi, T. Ikariya, *J. Am. Chem. Soc.* **2007**, *129*, 290–291; h) M. Ito, A. Osaku, A. Shiibashi, T. Ikariya, *Org. Lett.* **2007**, *9*, 1821–1824; i) R. J. Lundgren, M. A. Rankin, R. McDonald, G. Schatte, M. Stradiotto, *Angew. Chem. Int. Ed.* **2007**, *46*, 4732–4735.

[6] G. Zassinovich, G. Mestroni, S. Gladiali, *Chem. Rev.* **1992**, *92*, 1051–1069.

[7] a) D. A. Alonso, P. Brandt, S. J. M. Nordin, P. G. Andersson, *J. Am. Chem. Soc.* **1999**, *121*, 9580–9588; b) M. Yamakawa, M. Ito, R. Noyori, *J. Am. Chem. Soc.* **2000**, *122*, 1466–1478.

[8] a) R. L. Chowdhury, J. E. Bäckvall, *J. Chem. Soc., Chem. Commun.* **1991**, 1063–1064; b) A. Aranyos, G. Csjernyik, K. J. Szabó, J. E. Bäckvall, *Chem. Commun.* **1999**, 351–352; c) O. Pámies, J. E. Bäckvall, *Chem. Eur. J.* **2001**, *7*, 5052–5058; d) J. R. Fulton, A. W. Holland, D. J. Fox, R. G. Bergman, *Acc. Chem. Res.* **2002**, *35*, 44–56; e) H. E. Bryndza, W. Tam, *Chem. Rev.* **1988**, *88*, 1163–1188.

[9] a) W. Baratta, G. Chelucci, S. Gladiali, K. Siega, M. Toniutti, M. Zanette, E. Zangrando, P. Rigo, *Angew. Chem. Int. Ed.* **2005**, *44*, 6214–6219; b) W. Baratta, K. Siega, P. Rigo, *Chem. Eur. J.* **2007**, *13*, 7479–7486.

[10] P. E. Garrou, *Chem. Rev.* **1981**, *81*, 229–266.

[11] H. P. Fritz, I. R. Gordon, K. E. Schwarzhans, L. M. Venanzi, *J. Chem. Soc.* **1965**, 5210–5216.

[12] a) D. C. Mudalige, S. J. Rettig, B. R. James, W. R. Cullen, *J. Chem. Soc., Chem. Commun.* **1993**, 830–832; b) D. C. Muda-

lige, E. S. Ma, S. J. Rettig, B. R. James, W. R. Cullen, *Inorg. Chem.* **1997**, *36*, 5426–5427; c) E. S. F. Ma, S. J. Rettig, B. R. James, *Chem. Commun.* **1999**, 2463–2464; d) C. B. Pamplin, E. S. F. Ma, N. Safari, S. J. Rettig, B. R. James, *J. Am. Chem. Soc.* **2001**, *123*, 8596–8597.

[13] L. Dahlenburg, C. Kühnlein, *J. Organomet. Chem.* **2005**, *690*, 1–13.

[14] a) J. P. Jesson in *Transition Metal Hydrides*, (Eds: E. L. Muetterties), Marcel Dekker, New York, **1971**, p., 87; b) J. T. Poulton, M. P. Sigalas, K. Folting, W. E. Streib, O. Eisenstein, K. G. Caulton, *Inorg. Chem.* **1994**, *33*, 1476–1485.

[15] a) P. Chen, *Angew. Chem. Int. Ed.* **2003**, *42*, 2832–2847; b) P. Pelagatti, M. Carcelli, F. Calbiani, C. Cassi, L. Elviri, C. Pelizzi, U. Rizzotti, D. Rogolino, *Organometallics* **2005**, *24*, 5836–5844; c) C. K. Ralph, R. J. Hamilton, S. H. Bergens "A Tour Guide to Mass Spectrometric Studies of Hydrogenation Mechanism" in *Handbook of Homogeneous Hydrogenation* (Eds: J. G. deVries, C. J. Elsevier) Wiley-VCH, Weinheim, **2007**, vol. 1, p. 359.

[16] a) M. Yamakawa, I. Yamada, R. Noyori, *Angew. Chem. Int. Ed.* **2001**, *40*, 2818–2821; b) R. Noyori, M. Yamakawa, S. Hashiguchi, *J. Org. Chem.* **2001**, *66*, 7931–7944; c) P. Brandt, P. Roth, P. G. Andersson, *J. Org. Chem.* **2004**, *69*, 4885–4890; d) A. Comas-Vives, G. Ujaque, A. Lledós, *Organometallics* **2007**, *26*, 4135–4144; e) D. G. I. Petra, J. N. H. Reek, J. W. Handgraaf, E. J. Meijer, P. Dierkes, P. C. Kamer, J. Brussee, H. E. Schoemaker, P. W. N. M. van Leeuwen, *Chem. Eur. J.* **2000**, *6*, 2818–2829.

[17] J. Tomasi, B. Mennucci, R. Cammi, *Chem. Rev.* **2005**, *105*, 2999–3094.

[18] W. J. Hehre, L. Radom, P. van R. Schleyer, J. A. Pople in *Ab Initio Molecular Orbital Theory*, Wiley-Interscience, **2005**.

[19] Any attempts made to isolate the neutral complex {Ru[(κ^2P,N)PNH](*p*-cymene)Cl} (**X**) were unsuccessful.

[20] For the construction of **TS3** we fixed the configuration on ruthenium as (*S*) and approached the ketone by the two different enantiofaces, *Re* and *Si*. DFT calculations evidence two different energetic profiles, and the *Si* face was favored over the *Re* face (23.8 and 27.2 kcal/mol with respect to the previous step). The found energy differences (3.4 kcal/mol) arise from specific C–H(*p*-cymene)–π(phenyl)interactions that are possible only when the ketone approaches ruthenium from the *Si* face. This enantioface discrimination was invoked at the origin of the observed high enantioselectivity found with Noyori's catalysts. However, because **V** is expected to be present as a racemate in solution, the choice of a precise configuration at metal and of a precise enantioface of the ketone is totally arbitrary (no asymmetric induction was observed with **1a**,**b**).

[21] The possibility that **TS3** could involve an *i*PrOH molecule, as described in J. W. Handgraaf, E. J. Meijer, *J. Am. Chem. Soc.* **2007**, *129*, 3099, was investigated by ab initio calculations. In particular, we searched saddle points after the introduction of one explicit molecule of *i*PrOH bridging acetophenone and the NH_2 functionality of **V** through hydrogen bonds. This led to a stable transition state with only one imaginary frequency describing synchronous hydrogen transfer from NH_2 and Ru–H functionalities. Preliminary calculations show a sensible destabilization in energy of **TS3**.

[22] a) R. Noyori, S. Hashiguchi, *Acc. Chem. Res.* **1997**, *30*, 97–102; b) I. M. Pastor, H. Adolfsson, *Chem. Commun.* **2002**, 2046; c) A. Bøgevig, I. M. Pastor, H. Adolfsson, *Chem. Eur. J.* **2004**, *10*, 294–302.

[23] O. Herd, A. Heßler, M. Hingst, M. Tepper, O. Stelzer, *J. Organomet. Chem.* **1996**, *522*, 69–76.

[24] After elution of the ligand, a red band remained at the head of the column that was eluted by diethyl ether. By slow evaporation of the solvent, red crystals suitable for X-ray analysis were obtained. Crystal system: tetragonal, space group: I 4_1/a, a = 21.596(6) Å, c = 32.376(9) Å. $^{31}P\{^1H\}$ NMR ($CDCl_3$): δ = 75 (br. s, Ph_2PNH), 9 (br. s, PPh_3) ppm; see Supporting Information.

[25] D. R. Coulson, *Inorg. Synth.* **1990**, 107–109.

[26] M. A. Bennet, T. N. Huang, T. W. Matheson, A. K. Smith, *Inorg. Synth.* **1982**, 74–78.

[27] PLATON An Integrated Tool for the Analysis of the Results of a Single-Crystal Structure Determination: A. L. Speck, *Acta Crystallogr., Sect. A* **1990**, *46*, C34.

[28] A Semiempirical Method of Absorption Correction A. C. T. North, D. C. Phillips, F. Scott Mathews, *Acta Crystallogr., Sect. A* **1968**, *24*, 351.

[29] P. T. Beurskens, G. Beurskens, R. Gelder, S. Garcia-Granda, R. O. Gould, R. Israel, J. M. M. Smits, *The DIRDIF-99 Program System,* Crystallography Laboratory, University of Nijmegen, The Netherlands, **1999**.

[30] a) W. H. Zachariasen, *Acta Crystallogr.* **1967**, *23*, 558; b) A. C. Larson in *The Inclusion of Secondary Extinction in Least-Squares Refinement of Crystal Structures – Crystallographic Computing* (Eds F. R. Ahmed, S. R. Hall, C. P. Huber) Munksgaard, Copenhagen, **1970**, p. 291.

[31] a) D. T. Cromer, J. B. Mann, *Acta Crystallogr., Sect. A* **1968**, *24*, 321; b) D. T. Cromer, J. B. Mann, *International Tables for X-ray Crystallography* Kynoch Press, Birmingham **1974**. vol. IV, p. 55.

[32] D. T. Cromer, D. Liberman, *J. Chem. Phys.* **1970**, *53*, 1891–1898.

[33] S. R. Hall, D. J. du Boulay, R. Olthof-Hazekamp (Eds.), *XTAL3.7 System*. University of Western Australia, **2000**.

[34] a) *SAINT: SAX, Area Detector Integration*, Siemens Analytical instruments INC., Madison, Wisconsin, USA; b) G. Sheldrick, *SADABS: Siemens Area Detector Absorption Correction Software*, University of Goettingen, Germany, **1996**.

[35] A. Altomare, M. C. Burla, M. Cavalli, G. Cascarano, C. Giacovazzo, A. Guagliardi, A. G. Moliterni, G. Polidori, R. Spagna, *Sir97: A New Program For Solving and Refining Crystal Structures*, Istituto di Ricerca per lo Sviluppo di Metodologie Cristallografiche CNR, Bari, **1997**.

[36] G. Sheldrick, *SHELXL97: Program for Structure Refinement*, University of Goettingen, Germany, **1997**.

[37] L. J. Farrugia, *J. Appl. Crystallogr.* **1999**, *32*, 837–838.

[38] M. Nardelli, *J. Appl. Crystallogr.* **1995**, *28*, 659.

[39] a) F. H. Allen, O. Kennard, R. Taylor, *Acc. Chem. Res.* **1983**, *16*, 146–153; b) I. J. Bruno, J. C. Cole, P. R. Edgington, M. Kessler, C. F. Macrae, P. McCabe, J. Pearson, R. Taylor, *Acta Crystallogr., Sect. B* **2002**, *58*, 389–397.

[40] a) A. D. Becke, *J. Chem. Phys.* **1993**, *98*, 5648–5652; b) C. Lee, W. R. G. Yang, *Phys. Rev. B* **1988**, *37*, 785–789; c) P. J. Stephens, F. J. Devlin, C. F. Chabalowski, M. J. Frisch, *J. Phys. Chem.* **1994**, *98*, 11623–11627.

[41] M. J. Frisch, G. W. Trucks, H. B. Schlegel, G. E. Scuseria, M. A. Robb, J. R. Cheeseman, J. A. Montgomery Jr, T. Vreven, K. N. Kudin, J. C. Burant, J. M. Millam, S. S. Iyengar, J. Tomasi, V. Barone, B. Mennucci, M. Cossi, G. Scalmani, N. Rega, G. A. Petersson, H. Nakatsuji, M. Hada, M. Ehara, K. Toyota, R. Fukuda, J. Hasegawa, M. Ishida, T. Nakajima, Y. Honda, O. Kitao, H. Nakai, M. Klene, X. Li, J. E. Knox, H. P. Hratchian, J. B. Cross, V. Bakken, C. Adamo, J. Jaramillo, R. Gomperts, R. E. Stratmann, O. Yazyev, A. J. Austin, R. Cammi, C. Pomelli, J. W. Ochterski, P. Y. Ayala, K. Morokuma, G. A. Voth, P. Salvador, J. J. Dannenberg, V. G. Zakrzewski, S. Dapprich, A. D. Daniels, M. C. Strain, O. Farkas, D. K. Malick, A. D. Rabuck, K. Raghavachari, J. B. Foresman, J. V. Ortiz, Q. Cui, A. G. Baboul, S. Clifford, J. Cioslowski, B. B. Stefanov, G. Liu, A. Liashenko, P. Piskorz, I. Komaromi, R. L. Martin, D. J. Fox, T. Keith, M. A. Al-Laham, C. Y. Peng, A. Nanayakkara, M. Challacombe, P. M. W. Gill, B. Johnson, W. Chen, M. W. Wong, C. Gonzalez, J. A. Pople, *Gaussian 03* (revision C.02), Gaussian, Inc., Wallingford, CT, **2004**.

[42] Relevant bond lengths [Å] and angles [°] (CM = centroid of the *p*-cymene ring) for complexes **1a**·CH_2Cl_2, **1b**, and

1d·CH_2Cl_2. **1a**: Ru1–N1 2.125(3), Ru1–P1 2.3072(9), Ru1–Cl1 2.3936(9), Ru1–CM 1.714; N1–Ru1–P1 81.12(9), N1–Ru1–Cl1 82.0(1), P1–Ru1–Cl1 83.71(3), Cl1–Ru1–CM 127.3, N1–Ru1–CM 128.7, P1–Ru1–CM 135.4. **1b**: Ru1–N1 2.13(1), Ru1–P1 2.296(5), Ru1–Cl1 2.380(4), Ru1–CM 1.706; N1–Ru1–P11 81.1(4), N1–Ru1–Cl1 79.8(4), P1–Ru1–Cl1 85.4(2), CM–Ru1–Cl1 127.5, CM–Ru1–P1 133.4, CM–Ru1–N1 130.9. **1d**·CH_2Cl_2: Ru–N 2.146(2), Ru–P 2.3102(7), Ru–Cl1 2.3952(7), Ru–CM 1.717; N–Ru–P 81.49(7), N–Ru–Cl1 82.51(7), P–Ru–Cl1 84.75(3), Cl1–Ru–CM 126.4, N–Ru–CM 129.9, P–Ru–CM 133.9.

Received: May 22, 2008
Published Online: August 25, 2008

